

**STATIC AND DYNAMIC
CALIBRATIONS OF THE
NANOTEST AT NPL.**

G Aldrich-Smith & N.M. Jennett

**Materials Performance
National Physical Laboratory. UK.**

September 2004

Static and Dynamic Calibrations of the NanoTest at NPL.

G Aldrich-Smith & N.M. Jennett

Materials Performance,
Engineering and Process Control Division,
National Physical Laboratory.

EXECUTIVE SUMMARY

The NanoTest is an instrumented (nano)indentation system supplied by Micro Materials Ltd., Wrexham, U.K. This report describes the procedures used for both static and dynamic calibrations of the NanoTest at NPL.

Static calibrations for force, displacement, indenter area function, frame compliance are described. Dynamic calibrations for effective pendulum mass, damping coefficient and dynamic compliance are discussed.

This document describes current best practice, an updated version will be produced on completion of this project (~September 2005).

© Crown copyright 2004
Reproduced by permission of the Controller of HMSO

ISSN 1744-0262

National Physical Laboratory
Teddington, Middlesex, UK, TW11 0LW.

Extracts from this report may be reproduced provided
that the source is acknowledged and the extract
is not taken out of context

We gratefully acknowledge the financial support of the UK Department of
Trade and Industry (National Measurement System Policy Unit)

Approved on behalf of Managing Director, NPL,
by Dr M Gee, Knowledge Leader (Performance Materials Group),
Engineering and Process Control Division

Contents

EXECUTIVE SUMMARY	2
1. Equipment	6
1.1. Static Calibrations	8
1.2. Dynamic Calibrations	9
2. Test Environment	10
3. Calibrations	10
3.1. Static Calibrations	10
3.1.2. Displacement Calibration	11
3.1.3. Area Function	12
3.1.3.1. Berkovich (NPL indenter code JEV)	13
3.1.3.2. Conical, 90° cone angle, 5µm tip radius (NPL indenter code JFS)	14
3.1.4. Frame Compliance	15
3.1.5. Certified Reference Materials	16
3.2. Dynamic calibrations	17
3.2.1. Damping coefficient & effective pendulum mass	17
3.2.2. Instrument energy storage	21
3.2.4. Impact acceleration distance	23
3.2.5. Dynamic compliance	23
References	24
Acknowledgements	25
APPENDIX A: AC Magnetic Flux Density Measurements in NanoTest Laboratory	26
APPENDIX B: MicroTest Force Calibration Procedure	28
APPENDIX C: Indenter Area Function by AFM	30

List of Figures

Figure 1a. Typical Force-Displacement curve showing measured and derived parameters	6
Figure 1b. Schematic showing various displacements during indentation	6
Figure 2. Schematic of the NanoTest 600 pendulum.	7
Figure 3. Effects of uncorrected frame compliance on the force-displacement curve.	8
Figure 4. Bridge box tuning.	11
Figure 5. NanoTest displacement calibration schematic, plan view.	12
Figure 6. AFM image of the Berkovich indenter	13
Figure 7. Area Function of the Berkovich indenter	13
Figure 8. AFM image of the Conical indenter	14
Figure 9. Area Function of the Conical indenter	14
Figure 10. The Two Reference Material Method.	15
Material 1: Tungsten. Material 2: Fused silica.	15
Figure 11. Freely swinging pendulum: experimental set-up with external data capture.	18
Figure 12. Freely swinging pendulum: displacement vs time.	18
Figure 13. Damped SHM model fitted to experimental data.	20
Figure 14. Impacts and rebounds into Aluminium.	21
Figure 15. Experimental set-up for stored energy.	22
Figure 16. Deflection at coil position	22
Figure 17. Deflection at pivot springs	23
Figure B1. MicroTest force calibration schematic, side view	28
Figure B2: MicroTest force calibration.	29
Figure C1. Schematic of AFM z-calibration using a Jamin interferometer.	30
Figure C2. Matlab area function flowchart.	33

1. Equipment

The NanoTest is a pendulum based indentation system supplied by Micro Materials Ltd (Wrexham, UK). The NanoTest platform at NPL has both ‘Nano’ (NanoTest) and ‘Micro’ (MicroTest) indentation heads and a high-resolution microscope. A schematic of the NanoTest pendulum is given in Figure 2. A diamond indenter, mounted perpendicular to the vertical pendulum, is loaded against the sample by a coil and electromagnet situated on the opposing side of the pendulum pivot point. A capacitance plate system mounted directly behind the indenter measures displacement.

Force, displacement and time are recorded throughout the indentation cycle and the test sample modulus and hardness can be calculated using standard contact mechanics.

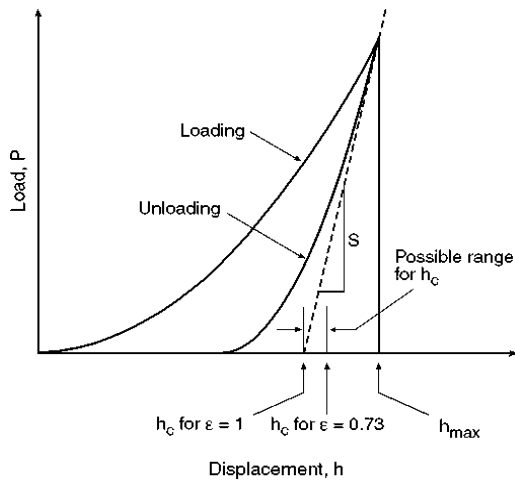


Figure 1a. Typical Force-Displacement curve showing measured and derived parameters

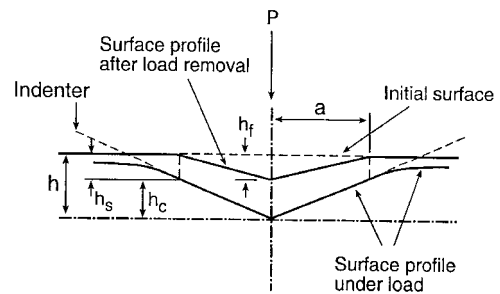


Figure 1b. Schematic showing various displacements during indentation

Using the Oliver and Pharr analysis [1] the stiffness of contact, S , equivalent to the reciprocal of the contact compliance can be related to modulus using:

$$E_R = \frac{\sqrt{\pi}}{2} \times \frac{1}{\sqrt{A_C}} \times \frac{1}{(C_T - C_F)} \quad \text{(Equation 1)}$$

where A_C is projected contact area at depth h_C , C_T is total compliance, and C_F is frame compliance. E_R is the reduced modulus of the diamond indenter and sample:

$$\frac{1}{E_R} = \left(\frac{1-\nu^2}{E} \right)_i + \left(\frac{1-\nu^2}{E} \right)_s \quad \text{(Equation 2)}$$

where i is for the diamond indenter and s is for the test sample.

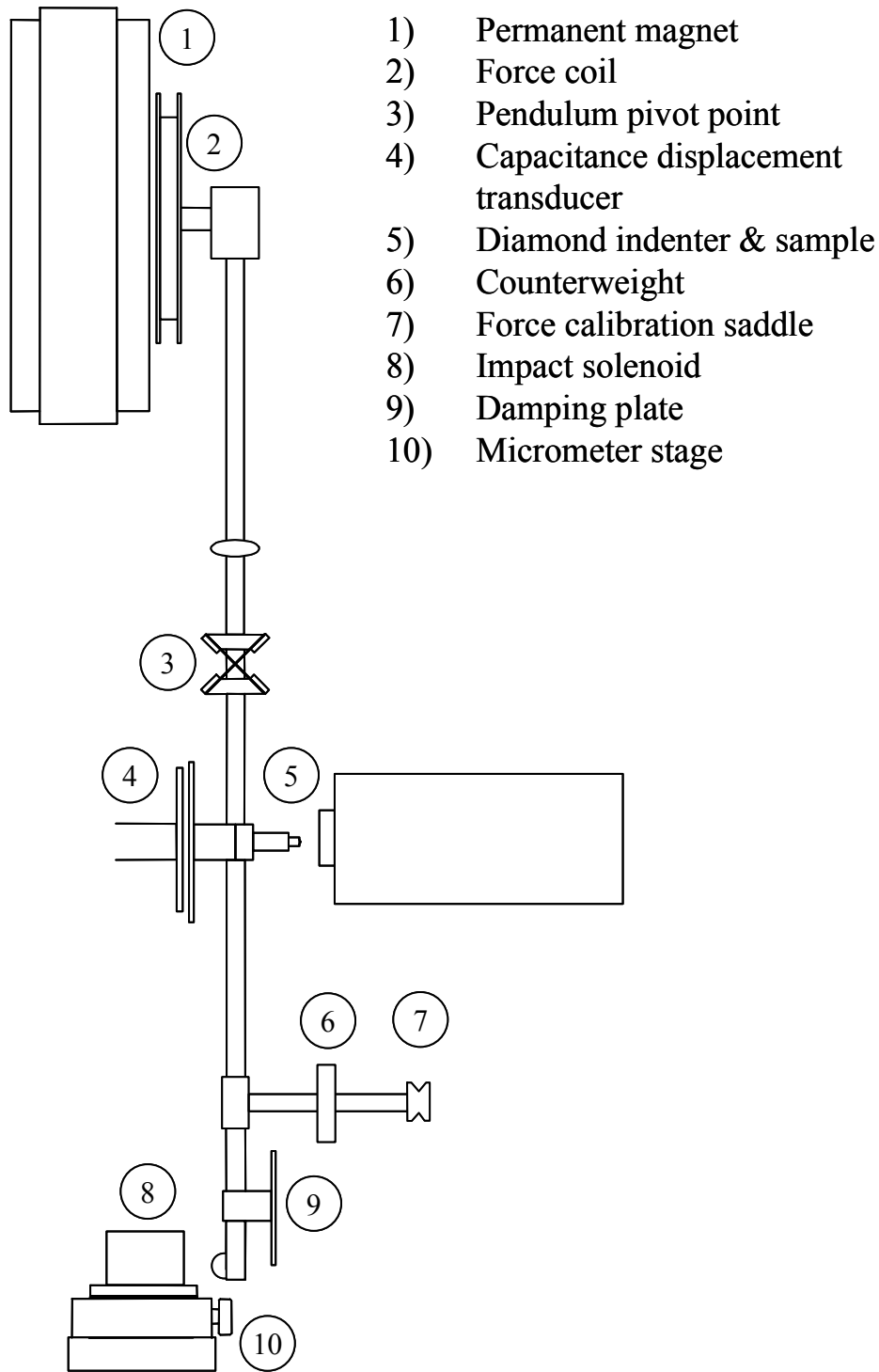


Figure 2. Schematic of the NanoTest 600 pendulum.
 (From *Micro Materials NanoTest User Guide* [2]).

Similarly, an accurate area function is important to obtain reproducible results between different machines and indenters. Often, however, the area function of an indenter is obtained indirectly by making indentations at only a few depths into a reference material. The inversion of the contact mechanics calculation yields a data set that is then fitted using a low order polynomial. In this case the “least squares fit” is often biased by small percentage but large absolute errors at large depths. In all cases, the paucity of data results in too few degrees of freedom in the fit and the rounding of the tip being poorly described. Even when data is taken at depths corresponding to the tip region, a poor choice of mathematical function may result in large area function errors due to inaccurate fitting at low indentation depths (A ‘least squares fit’ is only the ‘least’ for that particular function. The total sum of residuals to the fit will depend on the type of mathematical function chosen to fit the data). The lack of data may also disguise discontinuities in the area function of the indenter, e.g. due to damage, leading to an apparently inexplicable increase in the uncertainty of subsequent results.

1.2. Dynamic Calibrations

The starting point for calibrating the dynamic aspects of an instrumented indentation instrument is a full direct static calibration. Additional calibrations are then required for:

- Time stamps during data acquisition
- Effective mass of the impactor
- Damping coefficient of the pendulum
- Instrumental energy losses (e.g. Dynamic compliance, ringing, energy phase scattering, friction)

The core principle of nano-impact testing is that the velocity of the indenter can be measured continuously throughout the impact cycle via high-resolution measurement of displacement and time. The requirement for the calibration of the displacement time stamps is therefore clear. More subtle is the calibration of the effective mass and damping coefficient of the pendulum cum indenter system and the way that instrumental energy losses are affected not only by the impact velocity but also the indenter geometry and the material properties of the test piece.

In simple terms, the energy absorbed by the test piece is the difference between the kinetic energy of the indenter before and after impact (after correction for instrumental energy losses). For objects travelling in a straight line kinetic energy is

$$E = \frac{1}{2}mv^2 \quad (\text{Equation 3})$$

In reality the impacting body is a collection of rotating massive parts, all at different radii from the pivot point. An effective mass may be assigned, however, which is the mass that the indenter would have such that, when travelling in a straight line at the measured impact velocity, it has the same kinetic energy as the complicated pendulum system. The effective mass is related to the moment of inertia of the rotating system via its radius of gyration (the effective radius for the effective mass of the system if the mass was concentrated at a single point).

2. Test Environment

The NanoTest is located in Laboratory G2-L1 in the new NPL laboratory. It sits within a close-controlled temperature zone, set to $22^{\circ}\text{C} \pm 0.1^{\circ}\text{C}$. Temperature and humidity are logged continuously. A controlled constant temperature will help to reduce effects of any thermal drift during measurement.

The NanoTest is mounted on an anti-vibration table inside an acoustic enclosure to reduce the transmission of seismic and acoustic disturbances from the environment to the test data set. The NanoTest is currently mounted on a concrete block (~1300kg) on 4 IDE pneumatic isolators. As the indentation system is sensitive to horizontal vibrations it is planned to upgrade the vibration isolation to a 6-axis active controlled table in the near future.

As force is applied via a coil and electromagnet the AC magnetic flux density in various locations in G2-L1 was measured, this was found to be negligible, see Appendix A. It has been observed in other locations that the proximity of tube furnaces, distribution boards and other high power electrical equipment can generate significant AC magnetic fields.

3. Calibrations

The instrumented indentation standard, ISO 14577:1-3 [3] specifies the level of accuracy to be used in equipment calibrations. The NanoTest generally falls within the ‘Nano range’ where the indentation depth, $h \leq 200$ nm.

Test force and displacement should be calibrated with a minimum of 16 points equispaced over the calibration range for both force and displacement. Each calibration should be repeated a minimum of 3 times and with a recommended tolerance of $\pm 1\%$.

Indirect verification using certified reference materials (Section 3.1.5) should be undertaken before tests requiring high accuracy, with a suggested minimum interval of 1 week.

Frame compliance and indenter area function can also be indirectly measured via indentations into certified reference materials (CRMs) as well as by direct measurement techniques.

NPL are currently working with Micro Materials to produce an ISO 14577 compliant calibration package for the NanoTest.

3.1. Static Calibrations

Calibration routines for force and displacement are described. Indenter area function is measured using a metrological atomic force microscope (AFM). Frame compliance was inferred from indentations into a stiff certified reference material and using an AFM-derived indenter area function.

3.1.1. Force Calibration

Force calibration was performed using the Micro Materials method [2]. A series of small weights are hung from the saddle, see Figure 1, #7. This rotates the pendulum clockwise. The coil voltage is increased until the pendulum hangs vertically, as measured by the capacitance displacement transducer. The restoring force from the coil can be compared to the moment applied by the hanging weight.

This methodology requires the dimensions of the pendulum to be known precisely. A lower uncertainty force calibration method for the ‘Micro’ indenter uses a traceably calibrated load cell, as described in Appendix B. This is significantly quicker to perform and avoids the ISO requirement of 16 mass combinations [3]. A load cell with a suitable force range for the NanoTest is currently being investigated.

3.1.2. Displacement Calibration

The NanoTest uses a capacitive bridge circuit to measure displacement. The 4-element AC bridge circuit (5 kHz) consists of 3 adjustable controls in a bridge box and a capacitive displacement transducer, mounted directly behind the indenter, see Figure 2, #4. The bridge box is tuned before each test series performed (Figure 4), with the minimum voltage set to just above 0V and the limit stop voltage set to $\sim 8V$.

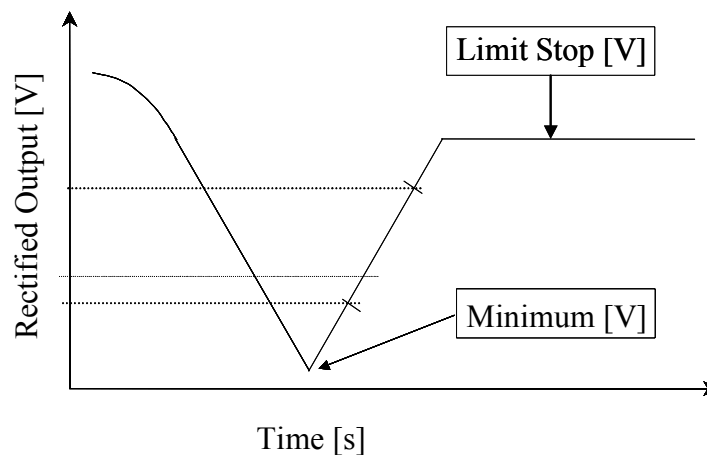


Figure 4. Bridge box tuning. Minimum is adjusted to just above 0V, Limit stop $\sim 8V$. The indentation test measurement range is shown between the dotted lines.

The capacitance displacement transducer was calibrated using an NPL differential plane (Jamin style) interferometer. A mirror was mounted on a ceramic rod and fixed to the XYZ stage. This was brought into contact with a 1mm diameter steel ball mounted as an indenter. Small movements of the stage then pushed the ceramic rod against the indenter and reduced the plate separation of the capacitance displacement transducer. The distance between the moving mirror and the reference mirror fixed to the NanoTest base plate was measured with a Jamin interferometer and used to calibrate displacement, see Figure 5.

The capacitive bridge Rectified Output [V] was converted to displacement using the existing calibration factor and plotted against Jamin Displacement [nm], this gradient allowing a new depth calibration factor to be calculated.

Analysis of fit residuals shows that the capacitance displacement transducer is slightly non-linear (residuals to a linear fit exceed $\pm 1\%$ at the extremities of the calibration range).

Changes in both temperature and humidity can give variations in the bridge box output, so a controlled environment is preferable.

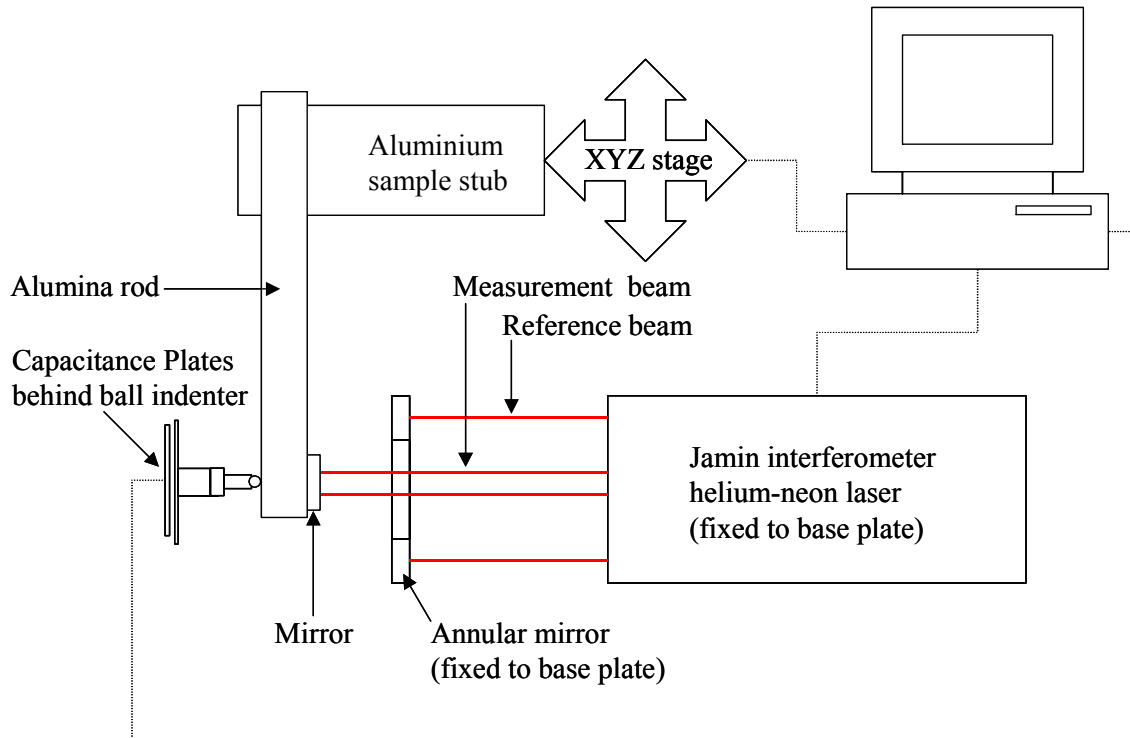


Figure 5. NanoTest displacement calibration schematic, plan view.

The bridge box was de-tuned, re-tuned, and a new depth calibration factor calculated. This procedure was repeated a total of 8 times by 2 operators. It was found that the depth calibration factor remained constant to within $\pm 0.8\%$.

3.1.3. Area Function

An indenter area function describes the shape of an indenter, giving a cross-sectional area (or contact area) as a function of depth, Figure 7. This is required to calculate modulus and hardness by instrumented indentation.

The area function was directly measured with a metrological atomic force microscope (AFM), traceably calibrated in X, Y & Z axes. AFM calibration and measurement is discussed in Appendix C. A Berkovich indenter (*NPL indenter code JEV*), purchased for a previous project, was used for characterising test materials for modulus and hardness by quasi-static nanoindentation.

Two indenters have been purchased for use in dynamic indentation testing:

- Sharp Rockwell, 120° cone angle, $25\mu\text{m}$ tip radius (*NPL indenter code JFT*)
- Conical, 90° cone angle, $5\mu\text{m}$ tip radius (*NPL indenter code JFS*)

Each indenter is given a unique identifier for internal quality procedures. The Area function is described as a function of depth (in 0.4 nm steps) using a b-spline for the tip apex and a linear fit for the far-field. Spline fits and linear far-field fits are coded into a MATLAB area function evaluation routine specific to each indenter measured.

Measurement of indenter area function by AFM is offered as an NPL measurement service.

3.1.3.1. Berkovich (NPL indenter code JEV)

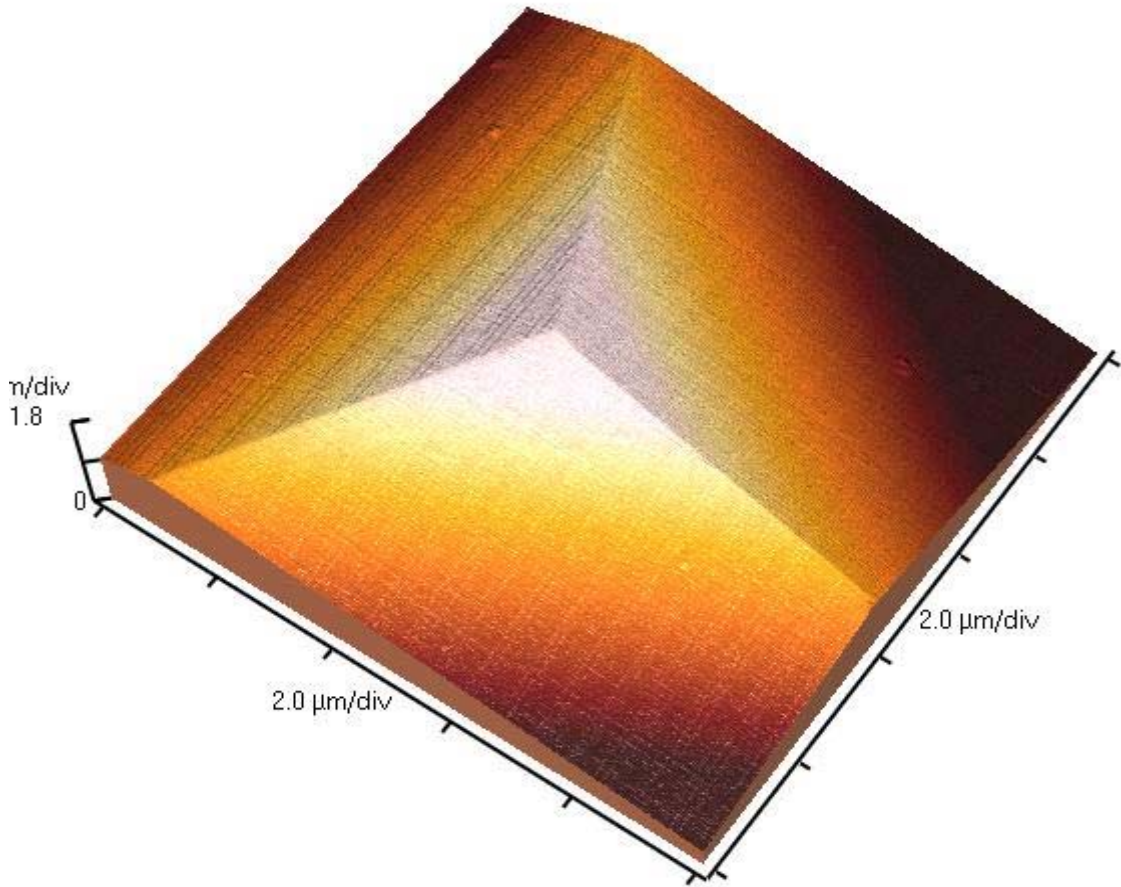


Figure 6. AFM image of the Berkovich indenter

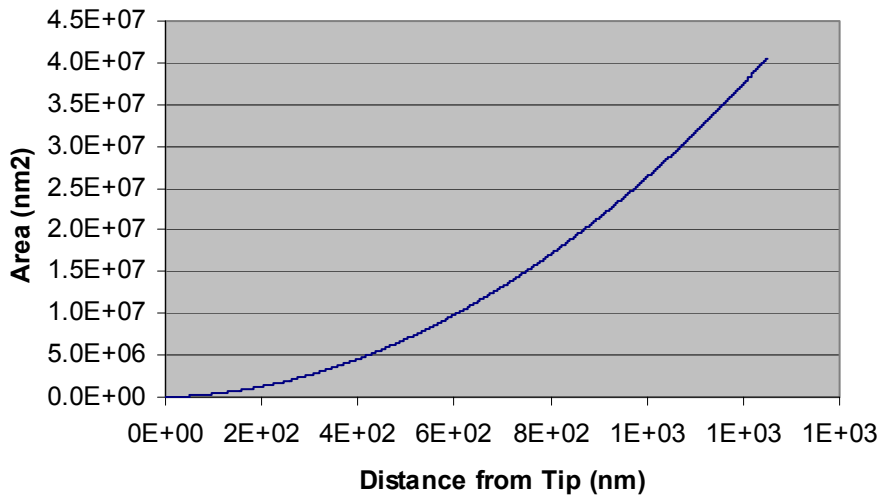


Figure 7. Area Function of the Berkovich indenter

3.1.3.2. Conical, 90° cone angle, 5µm tip radius (NPL indenter code JFS)

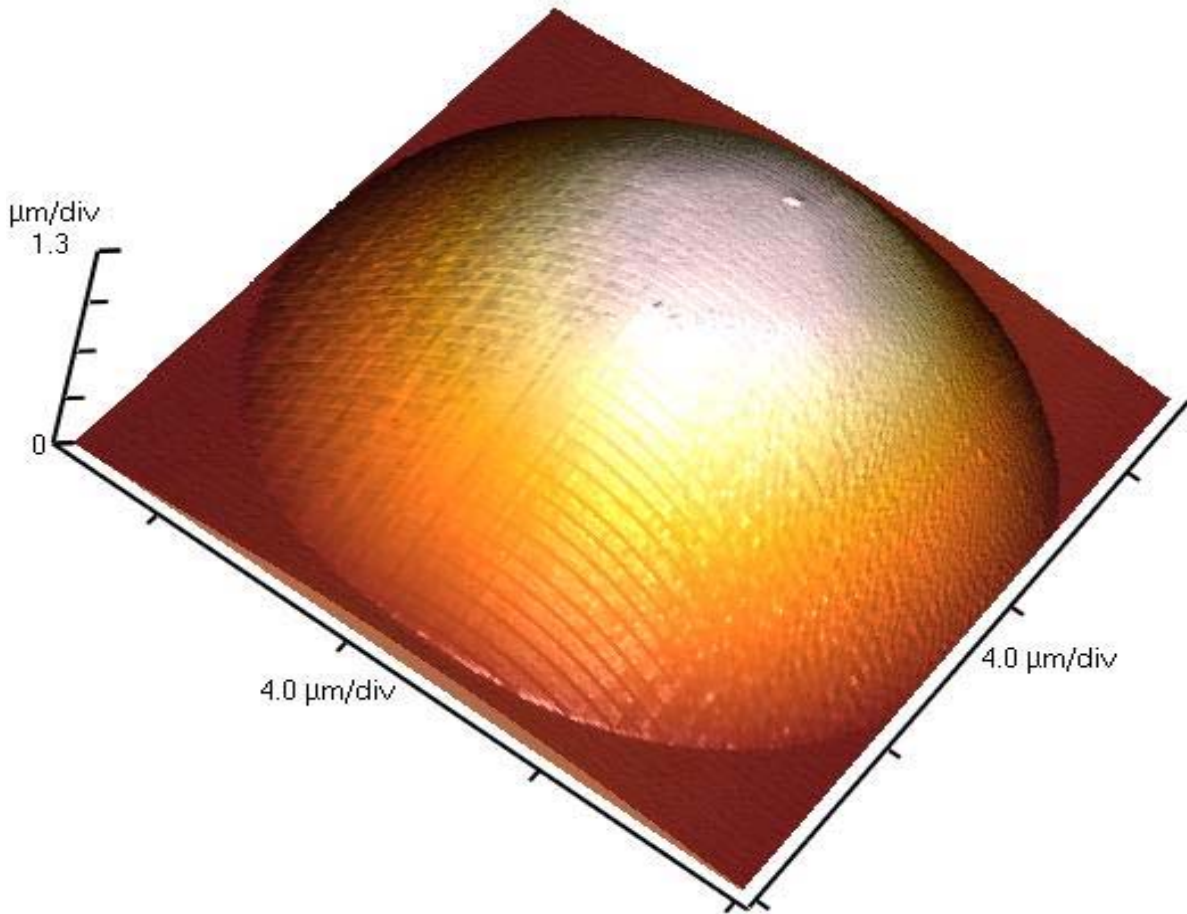


Figure 8. AFM image of the Conical indenter

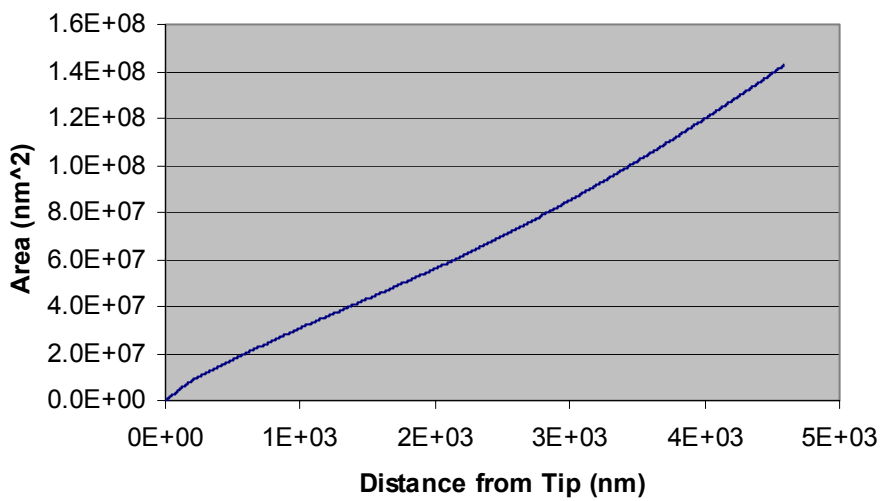


Figure 9. Area Function of the Conical indenter

The area function for the spherical indenter (NPL indenter code JFS), see Figure 9, can be recast as effective radius:

$$R_{EFF} = \frac{1}{2} \left[\frac{A}{\pi \cdot h} + h \right] \quad (\text{Equation 4})$$

where R_{EFF} is effective (instantaneous) radius of curvature and A is area.

3.1.4. Frame Compliance

The basic “two reference material” methodology developed by Herrmann *et al* [4] in the EU project, *INDICOAT* [5, 6], is shown in Figure 10, where C_t = total compliance and E_r = reduced modulus. Indentation data from two materials is used to calculate both frame compliance and indenter area function according to the procedure below.

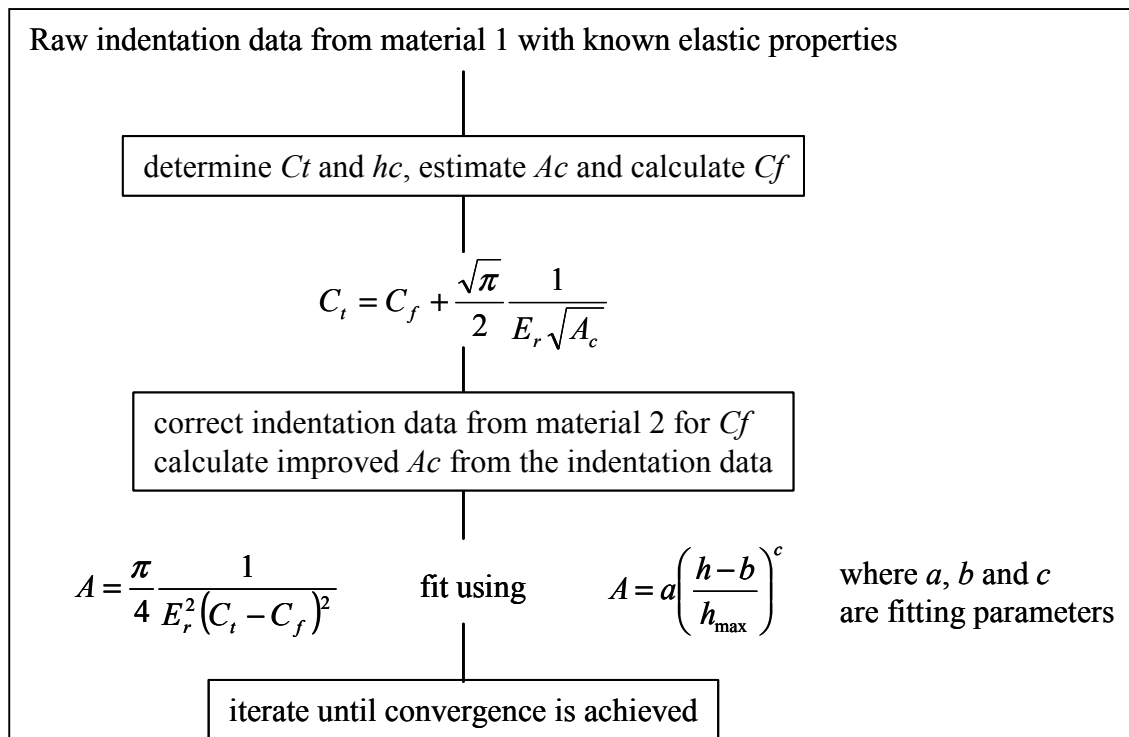


Figure 10. The Two Reference Material Method [4].

Material 1: Tungsten. Material 2: Fused silica.

The base line method is to use Tungsten and Fused Silica and assume only a reference value for the Fused Silica. To simplify the fitting of the area function required in the iterations, an alternative approach was taken. This was to fit $\sqrt{A_c}$ against h_c over the linear range of the data. Using this technique, it is essential to inspect the residuals of the fit to ensure that the h_c values being used are within the linear portion of the fit. This places a minimum value upon the range of valid h_c data. It was found that this method converged rapidly and repeatably on a single solution. However, the absolute values of area function and C_f obtained were dependent on the range of data fitted. Now, the compliance of a contact is proportional to $1/\sqrt{F_{\max}}$ and so the higher the forces used, the more reliable the determination of C_f . It was found that the uncertainty in the C_f value could be reduced by a factor of 3 if the maximum common depth in the data sets could be increased from $\sim 700\text{nm}$ to 1320 nm . This, however,

requires an F_{\max} of circa 220 mN in the tungsten and 400 mN in the Fused silica - a force at which cracking is observed.

A much lower uncertainty could be obtained if, instead of using a graphical method, a reference value was used for the Tungsten and the sample compliance, and therefore frame compliance, was calculated directly for each indentation. The averaging that was possible, either for replicate indents at each force or across all forces (i.e. assuming a force independent C_f) rapidly reduced the uncertainties in the mean C_f value obtained. The lowest uncertainty was obtained by using the arithmetic average and the widest range of data.

An alternative method for determining the frame compliance is to use the AFM area function and a reference value for the stiff certified reference material and directly calculate the sample compliance from the estimate of the contact area, A_c . C_f is then calculated by subtraction of the calculated sample compliance from the total measured compliance. This method has the lowest uncertainty for data limited to 100 mN and an equal uncertainty with the averaging method over the 400 mN data sets.

3.1.5. Certified Reference Materials

In order to comply with ISO 14577, and quality standards such as ISO 9001, organisations should be using certified reference materials, CRMs, to verify the calibration of instrumented indentation equipment. These can also be used for the indirect calibration in instrument frame compliance and indentation-derived area functions.

CRMs are designed to be a stable, reproducible, low uncertainty material. These have been extensively tested for homogeneity by indentation as a function of sample, indent location, and indentation depth. Modulus has also been confirmed by an independent technique.

A full calibration package for instrumented indentation equipment will need to:

- Verify that the machine is working properly
- Calibrate the area function of the indenter
- Validate the instruments frame compliance

However, CRMs have applications beyond ISO compliance as they can be used as an easy route for the improvement of measurement accuracy. In conjunction with a Master Indenter they can be used for:

- Quality Control / Assurance (control charts)
- Instrument fault diagnosis
- Interlaboratory comparisons for acceptance testing
- Instrument uncertainty determination

An uncertainty budget allows users to tailor the accuracy of their indentation results to the appropriate levels, for instance it could show if improvement in vibration isolation or the purchase of a measurement service to measure indenter area function by AFM would give the most cost effective improvements.

A specification for certified reference materials was generated in the EU project *DESIRED* [7]. NPL is currently developing these materials for commercial release via instrumented indentation equipment vendors, including Micro Materials Ltd.

3.2. Dynamic calibrations

An instrumented indentation test consists of several stages: moving the sample into contact with the indenter, holding on the surface to measure thermal drift, increasing force to a maximum, holding at maximum force to observe creep, removing force, and coming out of contact with the sample [note: the NanoTest uses a hold period at 90% unload for thermal drift corrections]. Typically the force will be applied and removed in ~30 seconds, and so the test can be described as quasi-static.

The NanoTest can perform quasi-static and dynamic indentations. In dynamic tests the indenter is held out of contact with the sample before being accelerated towards it, striking the surface, and bouncing out of contact. Repetitive dynamic indentation is also known as nano-impact and has been employed to assess the durability of materials under dynamic loading.

The contact duration is in the order of 10ms. Measuring the rebound velocity compared to the velocity before impact gives a coarse idea of the energy absorbed in the impact. The dynamic hardness, H_D , can be considered as the energy loss per unit area (GPa).

A data acquisition program was written in LABView to supplement the NanoTest software. This reads the displacement transducer signal via a National Instruments PCMCIA DAQCard-6024E and can collect data up to 200,000 samples.second⁻¹, however actual data rate is currently limited to that from the Micro Materials electronics console.

A solenoid is used to capture the pendulum whilst force is applied via the coil, see Figure 2, #8, when the solenoid voltage is removed the pendulum is released. This voltage drop triggers the data acquisition. Work is ongoing to capture the pendulum after a single impact on the surface to avoid the complications in analysis from multiple impacts.

The force applied by the coil is constant during the test. Work is ongoing to instrument the system to record the force, either behind the sample or indenter, during impact.

3.2.1. Damping coefficient & effective pendulum mass

A damping system is used during quasi-static indentation for low load experiments. A damping plate mounted on the base plate is brought into close proximity (~50 μm) to the damping plate fixed to the pendulum (Figure 2, #9). This reduces pendulum oscillations during the sample approach and indentation phase of the experiments. The damping plate on the base plate is removed during impact testing.

The damping coefficient is a measure of damping from air resistance from the damping plate, coil former and pendulum, from pivot friction, and from eddy currents generated as the coil moves in relation to the permanent magnet.

The NPL NanoTest has an early model depth measurement board. This has a linearity issue with the rectified output when the depth signal went above 8 volts. This was caused by saturation of one of the amplification stages within the depth board itself. For this experiment the depth signal was measured using a lock-in amplifier that was phase locked to a 5 kHz reference signal from the MicroTest bridge box. The change in amplitude from the AC

displacement transducer was converted to a linear DC signal that was logged with the external data capture. This was calibrated against stage encoder displacement as similarly discussed in Section 3.1.2.

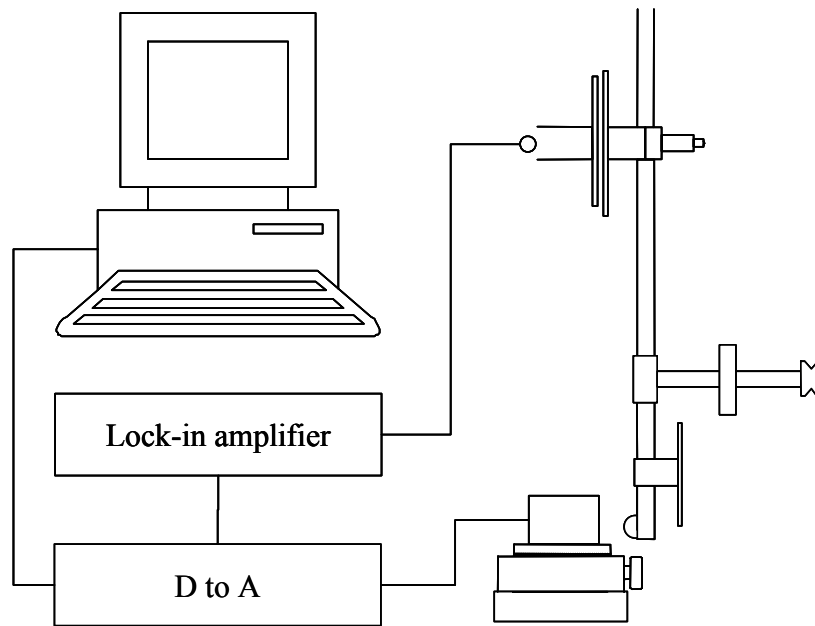


Figure 11. Freely swinging pendulum: experimental set-up with external data capture.

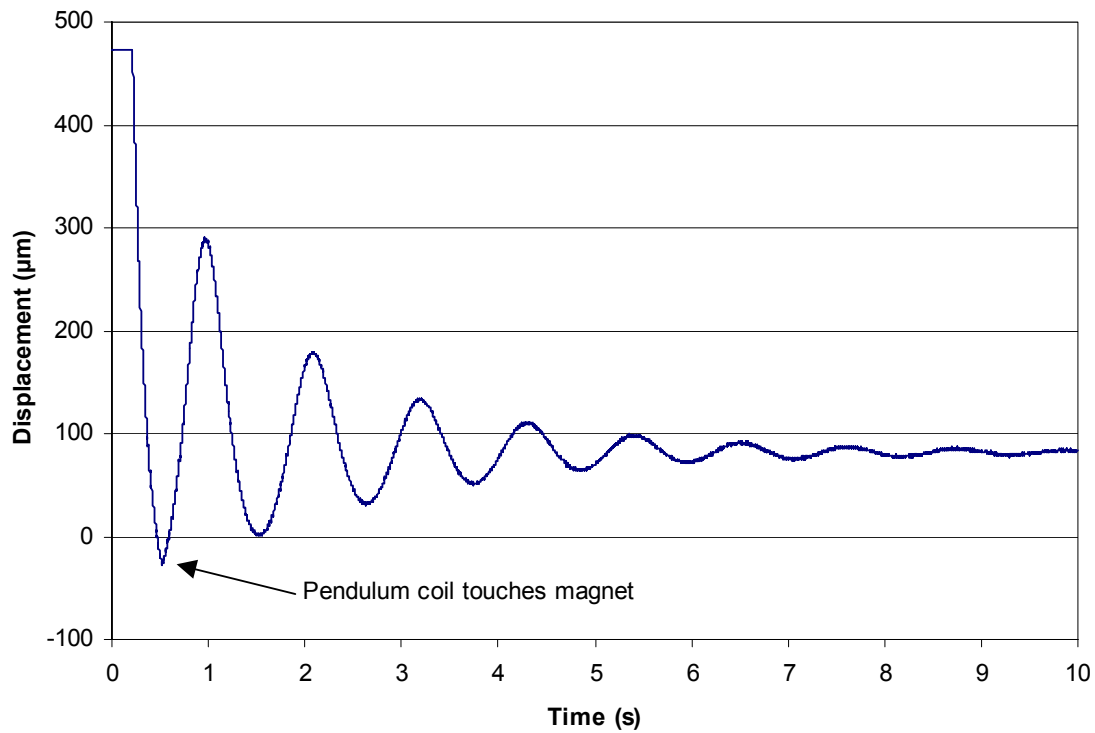


Figure 12. Freely swinging pendulum: displacement vs time.

The pendulum is held against the solenoid and the coil force holding it against the limit stop removed. When released from the solenoid the pendulum swings under gravity. The lock-in output was recorded using the LABView based data acquisition system, see Figure 11.

The pendulum was released from the solenoid at $t=0$ s (Figure 12) and the signal comes on scale at $t\sim 0.2$ s. The force coil (Figure 2, #2) bounces off the permanent magnet (Figure 2, #1) at $t\sim 0.5$ s, then swings freely until damping stops movement. This later part of the signal can be fitted using a damped simple harmonic motion model to find damping coefficient and effective pendulum mass.

To quantify the energy losses experienced by the pendulum during impact, it is essential to know both the effective mass of the impacting body and any damping that the system experiences as it accelerates into and rebounds from the target. This information can be obtained by measuring the response of the pendulum when swinging freely as a damped simple harmonic oscillator.

The solution to the equation of motion for damped simple harmonic motion ('s.h.m.') depends non-linearly on the parameters of amplitude, phase, frequency and damping factor. A MATLAB routine was written which used non-linear least squares solver and a standard Gauss-Newton optimisation algorithm to fit an under-damped simple harmonic oscillation model to the data. Ordinary differential equation for under-damped simple harmonic motion is:

$$\ddot{A}(t) + \frac{r}{m} \dot{A}(t) + \frac{s}{m} A(t) = 0 \quad (\text{Equation 5})$$

where $A(t)$ is amplitude of the swing as a function of time, t , and f is frequency of oscillation, r is the damping factor, s is the restoring force gradient, and m is the effective mass of the pendulum. The solution to the equation of motion is:

$$A(t) = e^{-Dt} (a \sin(2\pi ft) + b \cos(2\pi ft)) \quad (\text{Equation 6})$$

where:

$$2D = \frac{r}{m} \quad (\text{Equation 7})$$

and:

$$\frac{s}{m} = D^2 + (2\pi f)^2 \quad (\text{Equation 8})$$

where D is the amplitude decay time constant, and a & b are constants.

The above model, see Equation 5, assumes that the damping force is proportional to velocity, however it was found that this approximation began to break down for the higher velocities associated with the first couple of oscillations. The initial few seconds of data were therefore excluded from the fit. It was also found that the mean position of the oscillation was not constant with time. Given the short time-scale of the measurement and the large displacements involved, this was very unlikely to be a drift effect. The amplitude dependence of the effect suggested an additional damping force was being experienced by the system. This is possibly a "squeezed film damping" effect at the peak of the back swing, where the capacitor plate separation is very much reduced. As the swing amplitude reduces, the

minimum separation of the capacitor plates increases and the damping is less until the mean position of the swing asymptotes to the pendulum ‘at rest’ position. To prevent this effect distorting the results, an offset term was included as an additional parameter to allow for drift in the mean of the amplitude data.

It should be noted that the solution to the damped ‘s.h.m.’ equation only provides the ratio of the damping to the effective mass of the pendulum. Thus an additional calibration of the effective mass is required before the damping coefficient can be calculated.

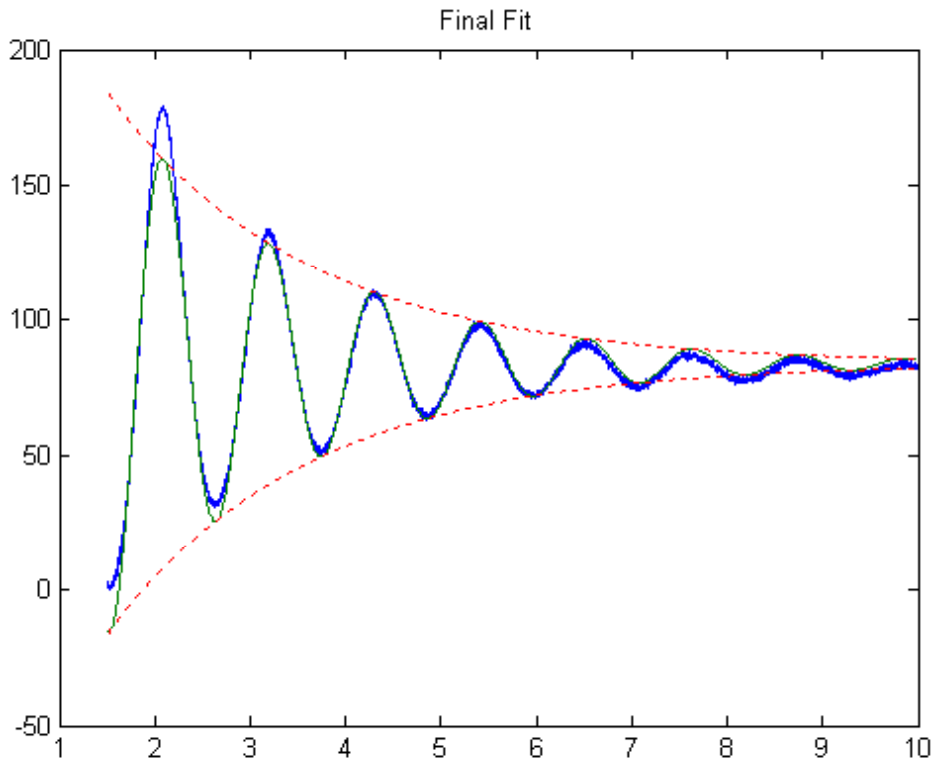


Figure 13. Damped SHM model fitted to experimental data (boundaries shown as dashed).

Effective mass of the pendulum was measured by performing a range of acceleration tests. The indenter was held on the solenoid and accelerated towards the sample with a range of forces from 1 to 10 mN and a distance of $\sim 10 \mu\text{m}$.

A 2nd order polynomial was fitted to the distance vs. time curve up to the first impact (0 sec to 0.6 sec in Figure 14). This was then double-differentiated to find the acceleration. The measurement was repeated for each accelerating force. The gradient of the force vs. acceleration is the pendulum mass. This is a reasonable first approximation. In reality, as soon as the pendulum starts to move, it will experience a damping component in addition to the inertia of the pendulum and this will reduce the measured acceleration. The effect of this is to increase the apparent effective mass. A refined technique is being developed to allow estimation or extrapolation of the measured acceleration to time =0 sec in order to remove the damping effects.

The value for effective mass can then be used, in conjunction with the damped simple harmonic motion solution, to back out the damping coefficient and effective pendulum length.

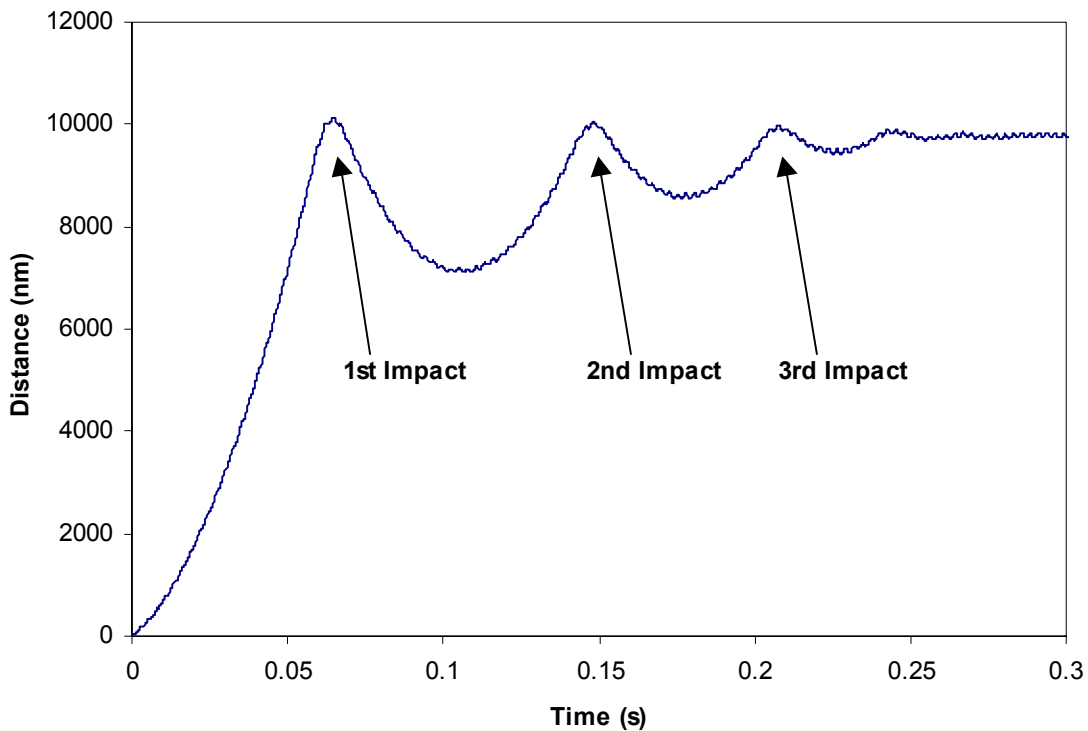


Figure 14. Impacts and rebounds into Aluminium, 1mN force, 10 μ m distance. Pendulum was released from solenoid at time=0 seconds.

3.2.2. Instrument energy storage.

Impact energy does not come solely from the loss of pendulum velocity during contact. Energy is stored in the pendulum prior to the solenoid release: the constant acceleration force applied by the coil creates deflection of the pendulum and compression of the pivot springs. This was measured as shown in Figure 15. The coil was energised using a variable power supply monitored with a digital voltmeter, and coil voltage converted to force using the calibration coefficient. Due to the pendulum geometry the force observed at the indenter is 2.5 times greater than that at the coil position. Pendulum deflection at the coil position and the pivot spring compression was measured using a fibre optic probe (MTI 2000 fonic sensor).

The pendulum is made from a ceramic rod, with material properties given in Table 1. Stored energy can then be calculated given the pendulum dimensions.

Table 1. Pendulum material properties.

Young's Modulus	330 GPa
Bulk modulus	228 GPa
Poisson's Ratio	0.22

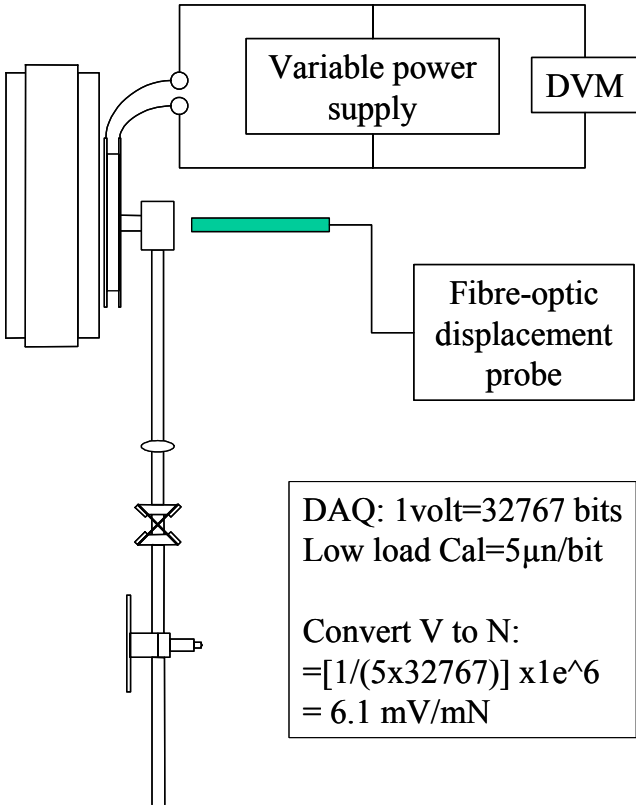


Figure 15. Experimental set-up for stored energy. Displacement was measured at the coil position and at the pivot.

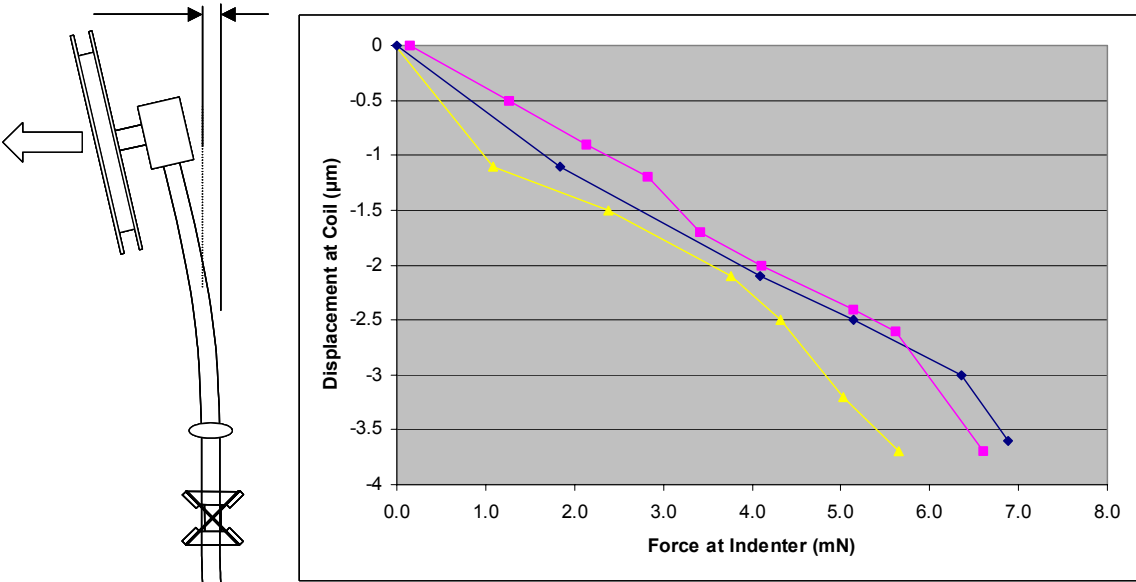


Figure 16. Deflection at coil position

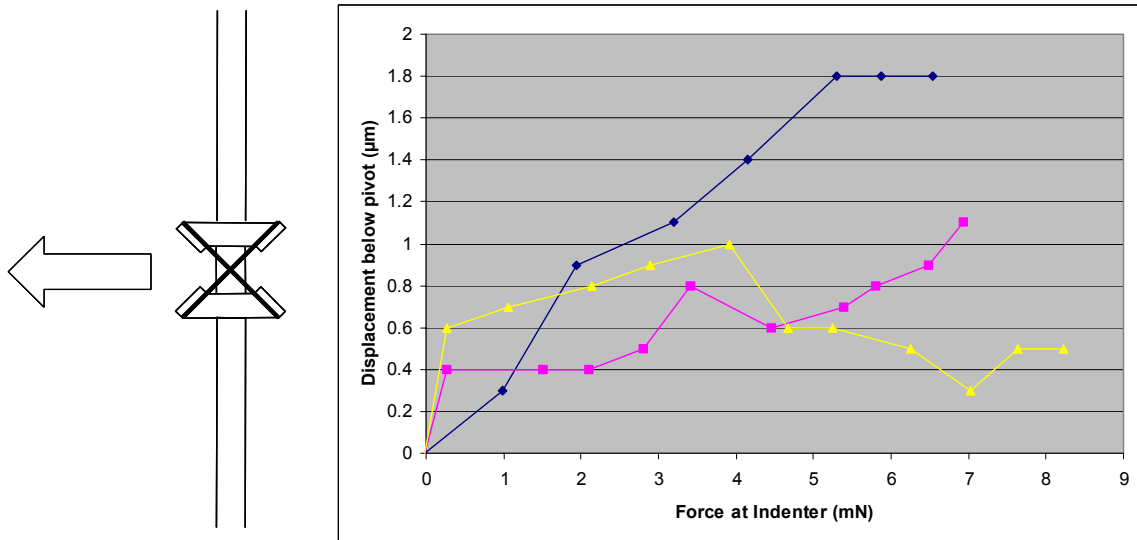


Figure 17. Deflection at pivot springs

3.2.4. Impact acceleration distance

Acceleration distance is set by moving the solenoid mounted on a micrometer stage, see Figure 2, #10. This is adjusted during the set-up of the impact tests. Displacement is measured at the indenter location using the capacitance transducer, calibrations of which are discussed in Section 3.1.2.

3.2.5. Dynamic compliance

As described previously dynamic hardness, H_D , can be considered as the energy loss per unit area, where

$$\text{Energy loss} = 0.5(\text{mass} \cdot V_{IN}^2) - 0.5(\text{mass} \cdot V_{OUT}^2)$$

where V_{IN} is pendulum velocity before impact and V_{OUT} is pendulum velocity after impact. However, energy loss to the sample does not just come from impact deformation, but from damping, ringing (elastic stress wave propagation), and dynamic compliance, i.e.,

$$\text{Energy loss} = \text{impact work} + \text{damping} + \text{ringing} + \text{dynamic compliance}$$

Dynamic compliance can be considered as the dynamic analogue of frame compliance, a force dependant displacement offset. This will be assessed later in the project by performing impacts on a perfectly elastic sample.

References

- [1] W. C. Oliver, G. M. Pharr, *J. Mater. Res.* **7**, 1564 (1992).
- [2] NanoTest 600 User Guide, Micro Materials Ltd., Wrexham, U.K.
- [3] ISO 14577. Metallic materials – Instrumented indentation test for hardness and materials parameters.
Part 1: Test method (2002)
Part 2: Verification and calibration of testing machines (2002)
Part 3: Calibration of reference blocks (2002)
Part 4: Properties of coatings (Committee Draft, expected 2006)
- [4] K. Herrmann, N.M. Jennett, W. Wegener, J. Meneve, K. Hasche and R. Seemann, *Thin Solid Films*, 377-378, (2000). p394-400.
- [5] N.M. Jennet et al, NPL Report MATC (A) 24 ‘Indicoat Final Report: Determination of Hardness and Modulus of Thin Films by Nanoindentation, NPL, UK, 2001.
- [6] Contract SMT4-CT98-2249 “*Determination of hardness and modulus of thin films and coatings by nanoindentation (INDICOAT)*”.
- [7] Contract G6RD-CT2000-00418 “*Development of Certified Reference Materials for Depth Sensing Indentation (DESIRED)*”.
- [8] EN 1071-3: 2001. Advanced technical ceramics – Methods of test for ceramic coatings – Part 3: Determination of adhesion by a scratch test.

Acknowledgements

This work was supported by the UK Government Department of Trade and Industry as part of the Measurements for Processability and Performance of Materials Programme (MPP). Many thanks to Micro Materials Ltd for software patches and useful discussions of results.

APPENDIX A: AC Magnetic Flux Density Measurements in NanoTest Laboratory

Measurements were made at 1m above floor level using a calibrated resultant indicating 3-axis magnetic field meter. A heater was used to simulate the planned 3 kW load in the laboratory and was located sufficiently far from the meter so as not to contribute to the reading. The heater was plugged into socket DB/L/3Y to the left of the back wall fixed laboratory benching. No other laboratories were loaded since this would be the case for the temporary use of the laboratory.

In the following tables the measured magnetic flux density values are shown for no load, see Table A1, and with a 3 kW load, see Table A2. The first row gives the X co-ordinate of the measurement point in meters and the first column the Y co-ordinate in meters. The zero reference of this grid is the left hand far corner when viewing the room from the door. The X co-ordinate corresponds to distances along the back wall and the Y coordinate to distances along the left wall.

All magnetic flux density values are in μT and distances in meters. In these tables, when the indicated reading exhibited scatter the maximum value is given in **red**.

Y/X	1	2	3
1	0.000	0.004	0.009
2	0.005	0.003	0.005
3	0.008	0.003	0.000
4	0.004	0.002	0.000
5	0.006	0.004	0.000

Table A1. Magnetic flux density values for no load.

Y/X	1	2	3
1	0.007	0.015	0.011
2	0.006	0.005	0.006
3	0.009	0.006	0.003
4	0.006	0.002	0.000
5	0.008	0.005	0.000

Table A2. Magnetic flux density values for a load of 3 kW.

For the purpose of comparison, the magnetic flux density in Laboratory F2 L6 at the bottom left hand corner of the first island bench is $0.036 \mu\text{T}$.

Also:

Magnetic flux density at the back of a powered Keithley 2000 DMM, $B = 0.4 \mu\text{T}$

Magnetic flux density at the back of a powered Analogue Associates $B = 2.0 \mu\text{T}$

MA 5000 amplifier with no current being driven.

For socket number 8 (DB/L/3Y) along X from the origin the probe head was placed in contact with the socket and 350 mm away.

In contact:

No load = $0.124 \mu\text{T}$

3 kW load = **$1.712 \mu\text{T}$**

350 mm away:

No load = 0.021 μT

3 kW load = 0.104 μT

With the heater plugged into the same socket, the magnetic flux density was measured at socket number 7 (DB/L/4Y) along Y from the origin.

In contact:

No load = 0.038 μT

3 kW load = 0.035 μT

The heater was then plugged into socket 1 (DB/L/4Y) along Y and the probe at socket 7 as before.

In contact:

No load = 0.038 μT

3 kW load = 1.972 μT

350 mm away:

No load = 0.029 μT

3 kW load = 0.070 μT

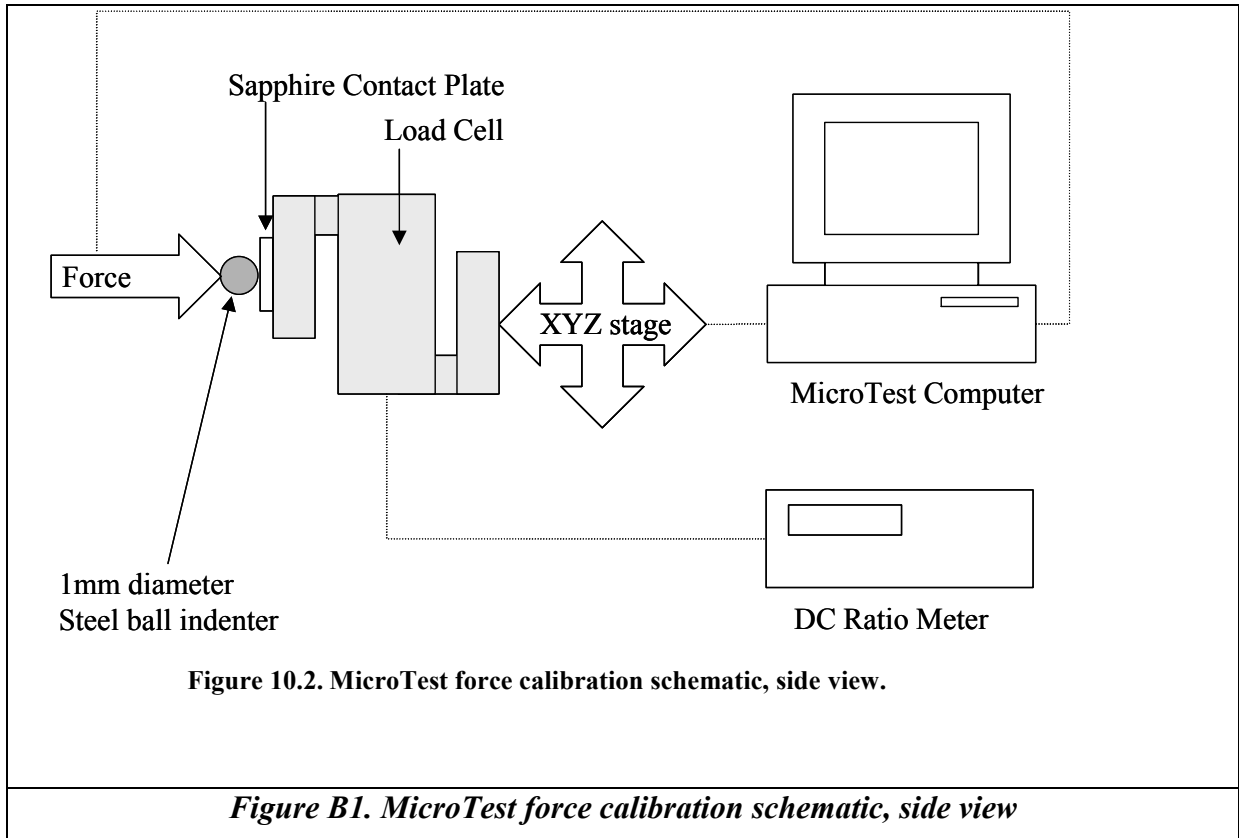
At position (X=2, Y=1) the maximum reading was observed with a load. Measurements were taken at this position with the laboratory lights turned off.

No load = 0.000 μT (0.004 μT with lights on)

3 kW load = 0.010 μT (0.015 μT with lights on).

APPENDIX B: MicroTest Force Calibration Procedure.

A 1mm diameter steel ball was mounted as an indenter and moved to close proximity with a load cell mounted on the XYZ stage, Figure B1. The load cell had been traceably calibrated at NPL and was read with a DC ratio meter. Calibration coefficients converted this voltage reading into mN.



A ‘multiple load cycle with increasing load’ test was programmed into the MicroTest software. This brought the indenter into contact with the load cell and increased the force from 500mN to 18500mN at $100\text{mN}\cdot\text{s}^{-1}$. Twenty-five equally spaced 35s hold intervals within this force range were used to allow the DC ratio meter reading to settle. This voltage reading was taken after 30s of each hold period. After the last hold period the force was removed at $400\text{mN}\cdot\text{s}^{-1}$. The MicroTest applied force was plotted against the load cell reading and the gradient used to adjust the MicroTest force calibrations. A check test was then performed. A software patch for easier control has subsequently been written for the software by Micro Materials.

The MicroTest software only allows for a linear force function to be used. However, inspection of the residuals to the fit clearly shows a 2nd order polynomial function, see Figure B2. This resulted in a usable force range of 3750mN to 18500mN, with forces below 3750mN being outside the $\pm 1\%$ linear fit residuals cut-off. An option to allow for a non-linear calibration factor in the software would avoid the need for post-processing to extend the useable calibration range.

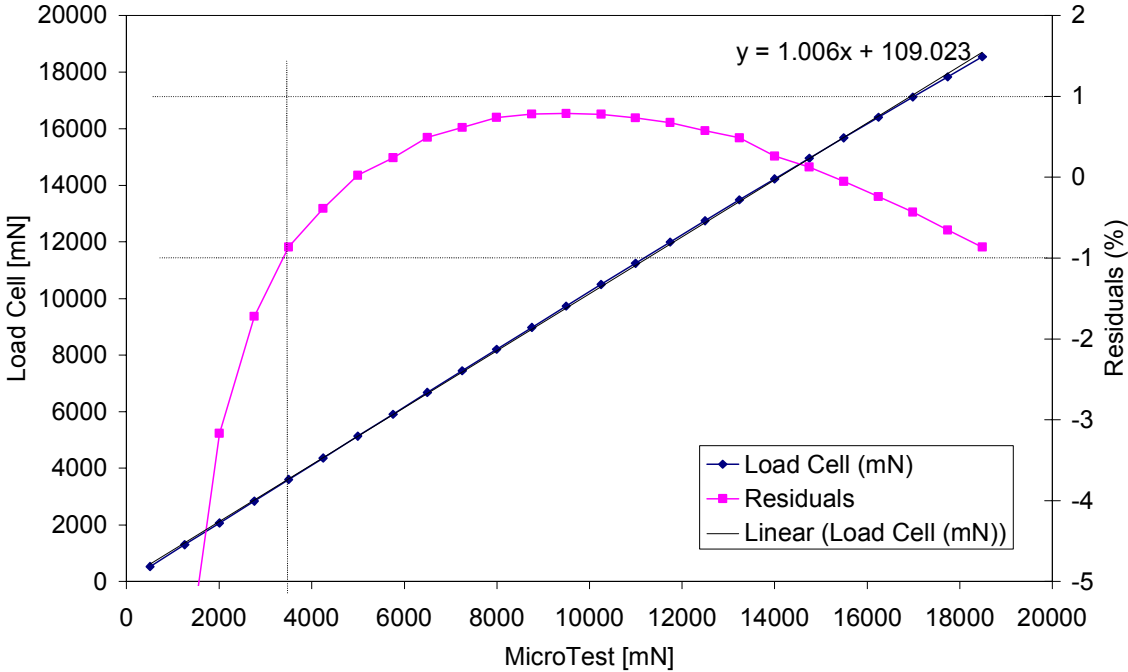


Figure B2: MicroTest force calibration showing the $\pm 1\%$ linear fit residuals cut-off suggested by ISO 14577.

APPENDIX C: Indenter Area Function by AFM

An indenter area function describes the shape of an indenter, giving a cross-sectional area (or contact area) as a function of depth. This is required to calculate modulus and hardness by instrumented depth sensing (nano)indentation. The area function was directly measured with a metrological atomic force microscope (AFM), traceably calibrated in X, Y & Z axes.

A Thermo-Microscopes (now Veeco) Autoprobe M5 AFM was used in contact mode for all measurements. This equipment moves the AFM tip with a piezo scanner rather than moving the sample under a fixed stylus. This allows for large or heavy items to be scanned over a $100\mu\text{m} \times 100\mu\text{m}$ scan area and $7.5\mu\text{m}$ depth range.

The M5 AFM has independent, linear, optical detectors on all axes (X, Y and Z). The ‘Scanmaster™’ feedback circuit uses the X and Y axes detectors to provide closed loop scan control. The detector on the z-axis eliminates errors due to piezo hysteresis from the z measurements. All axes can be traceably calibrated.

AFM Calibration

X and Y scanner movement was calibrated against a $2\mu\text{m}$ pitched silicon saw-toothed artefact previously calibrated at NPL. An $18\mu\text{m} \times 18\mu\text{m}$ scan was taken with orthogonal X and Y fast-scan directions over this artefact. The distance between 8 peaks was measured and compared to the certified value of $16\mu\text{m}$. The ratio of measured distance/calibrated distance was then used to update the scanner calibrations. Abbe errors were removed by scanning an optical flat and making this a reference plane to be automatically subtracted from all subsequent scans. Z calibration was performed using a Jamin type interferometer with a HeNe laser ($\lambda=633\text{nm}$). A mirror was mounted on top of the AFM scanner tube with the head inverted, see Figure C1. The piezo was then extended under manual software control and the change in distance between the moving mirror and a fixed reference mirror was measured using the Jamin interferometer. The ratio of measured distance/calibrated distance was then used to update the scanner calibrations.

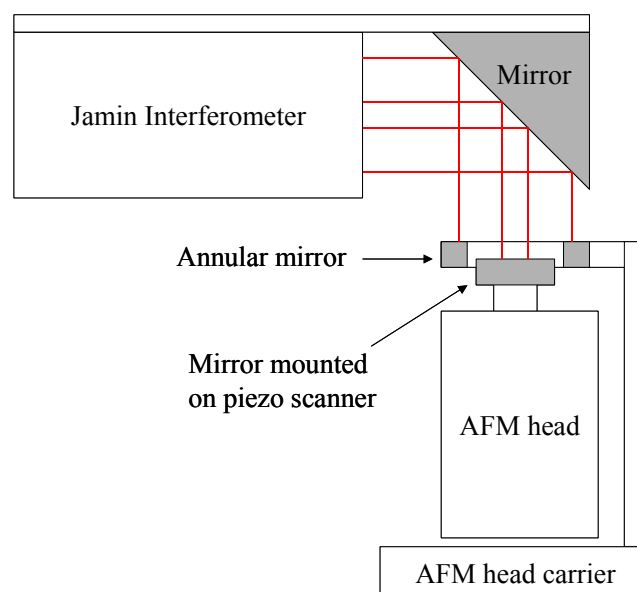


Figure C1. Schematic of AFM z-calibration using a Jamin interferometer.

Indenter Cleaning Protocol

Indenters were cleaned prior to AFM measurement to remove debris from the scan area. The cleaning procedures used gradually increased in severity. A microscope (magnification >200x) was used to check the indenter for damage and contamination after each stage:

1. Surface meniscus cleaning: dip an ~2mm diameter wooden stick vertically into alcohol, this picks up a droplet on the end. This droplet can be repeatedly brought into contact with the indenter tip. This removes fine dust from the indenter.
2. Clean with a cotton wool swab soaked with alcohol.
3. Polystyrene chip: break open an expanded polystyrene packing chip and dab the freshly exposed surface onto the indenter. Higher density foam chips work better.
4. Wipe/indent with wood: wipe the indenter towards the tip with a wooden stick (toothpick or similar). Also use low forces to push the stick onto the indenter. The stick can be dipped into alcohol before use.
5. Low load indentation into Al up to 2N: either use NanoTest to perform test indents or dead load the indenter manually. If loading manually, make sure that the sample does not move horizontally when in contact, Berkovich indenters damage easily when scratching. A modified sample press works well to apply loads vertically onto an indenter mounted in a plate or holder.
6. High load indentation into Al up to 20N: as a last resort only. The NPL Berkovich indenter withstood loads up to 20N without damage. Other indenters may not survive this step.
7. SiC paper: the ISO standard for scratch testing recommends cleaning Rockwell C indenters by abrading onto SiC paper [8]. This was not attempted.

To get the best finish on the indenter the cleaning steps were incrementally increased in severity then the steps were repeated in reverse order until sufficiently clean.

Indenter Measurement Routine

The diamond indenter was mounted normal to the AFM scan plane and initial scans were made to locate the indenter apex. The AFM cabinet was then closed to reduce noise and thermal drift. Continuous scans of the indenter were made, in both X and Y fast-scan directions, until analysis of the indenter apex location showed thermal drift had reached a minimum. This typically took 4-5 hours. The scans, alternating in X and Y as fast directions, also pushed any residual debris to the edge of the scan area.

AFM scan parameters were adjusted to suit each indenter, for the Berkovich indenter (NPL indenter code JEV) scan parameters were as following:

- 512 x 512 pixels
- 10 μ m x 10 μ m & 2 μ m x 2 μ m scan areas
- 1 line.s⁻¹ scan rate (i.e. 512 second duration)

Topography, error and z-detector images were recorded for both X and Y as fast scan directions.

Area Function Determination

The AFM records data files in a non-standard *.hdf format. These were imported into Matlab (Matlab v5.3, The Mathworks, US) using a custom written filter. A Matlab pixel counting software routine *AreaM5berk.m* was written to generate an area function (projected area vs. distance from tip) from the z-detector AFM files. The generation of the Berkovich area function is described below:

Area functions from the 2 μ m and 10 μ m scans were stitched together using an Excel spreadsheet that minimised the difference between the two functions over the h_c range of 50nm - 250nm. This gave an optimal 'composite' area function with high resolution at the indenter apex yet covering a large enough depth range for a reliable far-field fit.

A b-spline fit of this area function using appropriate parameters (23 interior knots between depths of 5nm to 1.2 μ m) was calculated using NPLFIT for both the X and Y fast-scan directions. NPLFIT is a public domain software suite developed by NPL to fit splines and polynomials to experimental data sets. The fit acts to smooth the dataset and to remove the need for an area function look-up table. The spline fit spanned the top 1.2 μ m of the indenter area function, in particular the apex, where the most deviation from a linear fit occurs. Previous work has shown that a 2nd or 3rd order polynomial is insufficient to describe the area function at the apex of an indenter. *AreaM5berk.m* also calculated a far-field fit to the AFM data for extrapolation to indentation depths greater than 1.2 μ m. The far-field fit was expressed as a linear function of $\sqrt{\text{Area}}$ vs. h_c .

Spline fits and linear far-field fits for both X and Y fast-scan directions were coded into a Matlab area function evaluation routine specific to each indenter measured. When the indentation analysis software submitted an h_c value an averaged contact area from both the X and Y fast scan fits was returned, Figure C2. This averaging further reduced both the influence of pixellation in the AFM data near the tip and any residual distortion due to thermal drift during the AFM scans. Alternatively the Matlab area function evaluation routine can be converted into an Excel spreadsheet add-in.

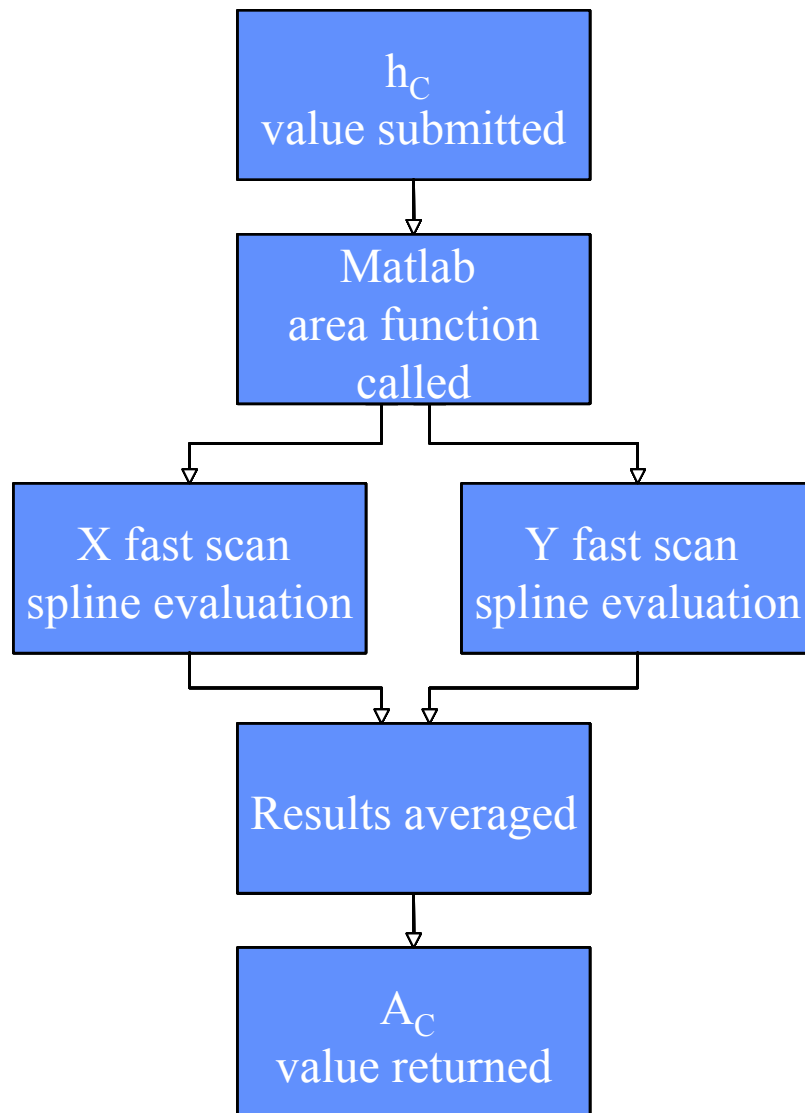


Figure C2. Matlab area function flowchart.

Input: Indentation depth, h_C ; Output: Contact area, A_C .